Protein Dynamics

Deutsche Ausgabe: DOI: 10.1002/ange.201501204
Internationale Ausgabe: DOI: 10.1002/anie.201501204

Kinetic Cooperativity in Human Pancreatic Glucokinase Originates from Millisecond Dynamics of the Small Domain**

*Mioara Larion, Alexandar L. Hansen, Fengli Zhang, Lei Bruschweiler-Li, Vitali Tugarinov, Brian G. Miller, and Rafael Brüschweiler**

Abstract: *The hallmark of glucokinase (GCK), which catalyzes the phosphorylation of glucose during glycolysis, is its kinetic cooperativity, whose understanding at atomic detail has remained open since its discovery over 40 years ago. Herein, by using kinetic CPMG NMR spectroscopic data for 17 isoleucine side chains distributed over all parts of GCK, we show that the origin of kinetic cooperativity is rooted in intramolecular protein dynamics. Residues of glucose-free GCK located in the small domain displayed distinct exchange behavior involving multiple conformers that are substantially populated ($p > 17\,\%$) with a k_{ex} value of $509 \pm 51\ s^{-1}$, whereas in the glucose-bound form these exchange processes were quenched. This exchange behavior directly competes with the enzymatic turnover rate at physiological glucose concentrations, thereby generating the sigmoidal rate dependence that defines kinetic cooperativity.*

The elucidation of mechanisms by which allostery and cooperativity are achieved in proteins for the regulation of their function remains fundamental, as it has important practical implications, for example, for the design of small-molecule activators and inhibitors. Human glucokinase (GCK), which is a 53 kDa monomeric enzyme, displays a special case of allosteric regulation known as kinetic cooperativity and has become a model system for the study of this phenomenon.[1,2] GCK acts as the primary glucose sensor in the human body. In the presence of adenosine triphosphate (ATP), it catalyzes the first step in glycolysis, which is the phosphorylation of glucose at the 6′-position.[3] The glucose concentration in the blood stream is precisely regulated through the sigmoidal response of the enzymatic rate of glucokinase to increasing glucose content; this effect is known as kinetic cooperativity (Figure 1 A).[1–3] The sigmoidal rate has its steepest slope at a glucose concentration in the low millimolar range that is close to the average glucose concentration in the blood stream (Figure 1 A, top). In this way, GCK can respond sensitively to increases in glucose concentration after the uptake of glucose-containing food, without completely depleting glucose levels.

Several X-ray crystal structures are available for the glucose-bound and the unliganded states of GCK. They exhibit, among other features, different opening angles between the large and the small domain (Figures 1 C and 3). In the bound form, GCK is closed and the protein segment with the amino acid sequence 151–179 forms a β-hairpin that stabilizes glucose at its binding site (PDB ID: 3IDH).[4] By contrast, in the unliganded form (PDB ID: 1V4T),[5] GCK is open and amino acids 151–179 do not show electron density, thus indicating the formation of a disordered loop, which was characterized by NMR spectroscopy in solution.[6]

Advances in experimental techniques, accompanied by progress in biomolecular computation, have led to a more general view of protein structure in terms of conformational ensembles. This development has also influenced the formulation of mechanisms by which allostery is achieved thermodynamically, whereby small molecules control enzymatic function through the modulation of conformational distributions or population shifts,[7–10] thus expanding on classical models of allostery and binding cooperativity.[11,12]

Understanding of kinetic cooperativity must not only take into account the underlying conformational ensembles, but also the precise motional timescales involved,[13–19] because cooperativity is encountered for GCK only in the reaction velocity and not in substrate binding (GCK has only a single glucose-binding site) and is hence a kinetic rather than a thermodynamic phenomenon. Theoretical models proposed since the 1970s postulate that cooperativity depends upon the presence of multiple conformations that interconvert on timescales comparable to the turnover rate constant, which is approximately $60\ s^{-1}$ at room temperature and higher at elevated temperature. However, experimental evidence has remained sparse.[13–19]

Nuclear magnetic resonance (NMR) Carr–Purcell–Meiboom–Gill (CPMG) relaxation dispersion spectroscopic experiments provide quantitative information about enzyme dynamics for a better understanding of the role of dynamics

[*] Dr. M. Larion, Dr. A. L. Hansen, Dr. L. Bruschweiler-Li, Prof. Dr. R. Brüschweiler
Department of Chemistry and Biochemistry
The Ohio State University
100 West 18th Avenue, Columbus, OH 43210 (USA)
E-mail: bruschweiler.1@osu.edu
Dr. F. Zhang
National High Magnetic Field Laboratory
Tallahassee, FL 32306 (USA)
Dr. V. Tugarinov
Laboratory of Chemical Physics, National Institute of Diabetes and Digestive and Kidney Diseases, National Institutes of Health
Bethesda, MD 20892-0520 (USA)
Prof. Dr. B. G. Miller
Department of Chemistry and Biochemistry, Florida State University
Tallahassee, FL 32306 (USA)

[**] This research was supported by the American Heart Association (grant 12POST12040344 to M.L.), the NIH (grant 1R01K081358 to B.G.M.), and the NSF (grant MCB-1360966 to R.B.).

Supporting information for this article, including a complete description of the experimental procedures, is available on the WWW under http://dx.doi.org/10.1002/anie.201501204.

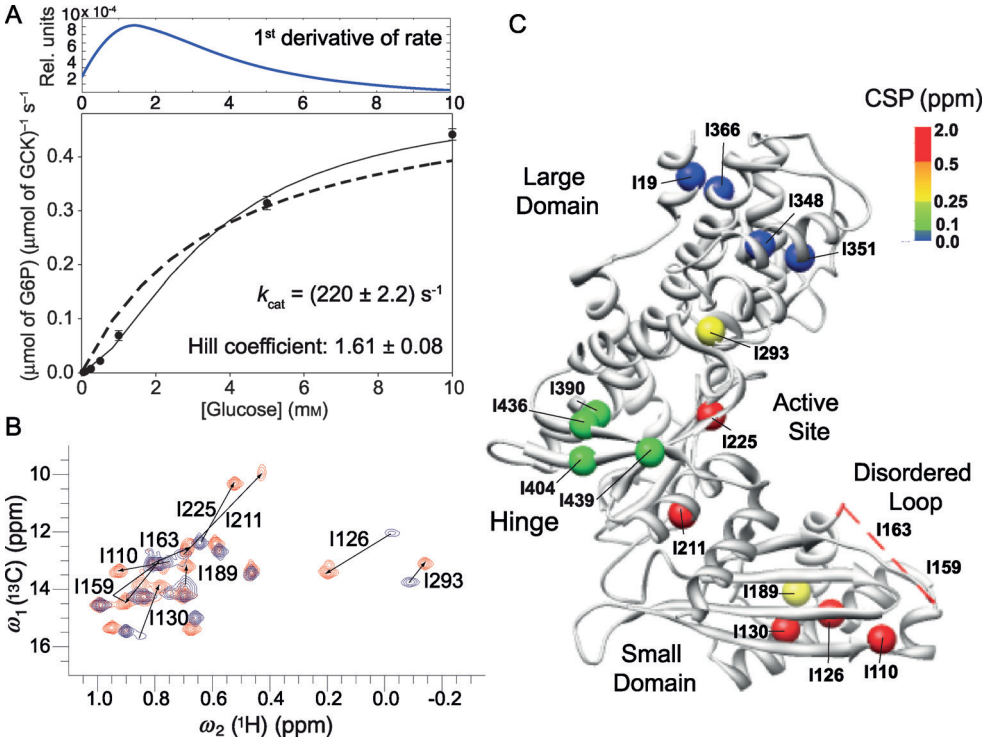

Figure 1. A) Kinetic-cooperativity profile of the enzyme glucokinase (GCK) during glucose phosphorylation at 313 K, which is the temperature used for all NMR spectroscopic experiments, with a turnover rate constant $k_{cat} = 220\ s^{-1}$. The first derivative of the fitted kinetic-cooperativity profile is plotted at the top. For comparison, a fit to Michaelis–Menten kinetics is indicated as a dotted line. B) Two-dimensional ^{1}H–^{13}C HMQC-TROSY spectra recorded at 700 MHz and 313 K of GCK labeled in the [^{13}C]methyl Ile δ1 position in the unliganded (blue) and glucose-bound form (red). Significant chemical-shift perturbations labeled with the corresponding amino acid number are indicated by arrows connecting cross-peaks belonging to the two states (see also Figure S2). C) X-ray crystal structure of unliganded GCK (PDB ID: 1V4T). The positions of all Ile methyl groups are mapped as spheres, which are colored according to the chemical-shift perturbation between unliganded and glucose-bound GCK, as indicated by the color scale.[5] The amino acid region 151–179, which lacks electron density in the unliganded structure and contains Ile-159 and Ile-163, is shown as a red dashed line.

for catalysis and regulation.[20–28] CPMG experiments report on motions occurring in the 100–2000 s^{-1} regime, which covers the timescales previously predicted to give rise to kinetic cooperativity.[13–19] For larger proteins, such as GCK, CPMG experiments can be applied to methyl groups of selectively labeled amino acids by taking advantage of their favorable spectroscopic properties in terms of sensitivity and line widths.[22] All 17 Ile side chains, which are ^{13}C-labeled in their δ1 methyl position, could be observed in the 2D ^{1}H–^{13}C HMQC-TROSY spectra[29] of the glucose-bound form, and they were previously assigned by site-selective mutagenesis. However, in the unliganded state, most of the residues of the small domain were undetectable. Their disappearance, which prevented more detailed analysis, was explained by the presence of conformational exchange on the millisecond timescale.[6]

Herein, we report the observation and quantification of the dynamics of all 17 Ile side chains in both the unliganded and the glucose-bound state of GCK by CPMG relaxation dispersion. These experiments were made possible by greater than 80% perdeuteration of the sample through the use of [D_8]glycerol as the sole carbon source and long induction times at 20 °C. Figure 1B shows the superposition of the 2D ^{1}H–^{13}C HMQC-TROSY spectra of GCK in the unliganded and glucose-bound forms with all isoleucine cross-peaks now observable in both states (see Figure S2 in the Supporting Information). The application of methyl-CPMG relaxation experiments[30] to $^{13}CHD_2$ groups at Ile δ1 positions in GCK in its unliganded and glucose-bound states led to the relaxation dispersion profiles depicted in Figure 2.

Residue-specific analysis of chemical-shift perturbations (CSPs) upon glucose binding showed that residues belonging to the same regions behaved similarly. Large-domain Ile residues, such as I19, I348, I351, and I366 (Figure 1C; see Figure S3), experienced very small ^{13}C chemical-shift changes, whereas hinge residues I390, I404, I436, and I439 displayed CSPs in the medium range (0.1–0.25 ppm). The most prominent CSPs were seen for residues located either in close vicinity to glucose, such as I211, I225, and I293, or in the small domain far from the glucose-binding site, such as I126, I130, I189, I110, I159, and I163 (0.25–2 ppm).

CPMG relaxation dispersion data also revealed differential behavior for residues belonging to the different regions. The strongest dispersions, as characterized by R_{ex}, the difference in effective relaxation rates ($R_{2,eff}$) at low and high CPMG refocusing frequencies, were found for the small-domain residues I126, I130, I189, and I211 of unliganded GCK ($R_{ex} = 5–60\ s^{-1}$; Figure 2A–C; see also Figure S4). Residues I110, I126, I130, I189, I211, and I293 could be globally fit to a two-state exchange model to yield $k_{ex} = k_{AB} + k_{BA} = 509 \pm 51\ s^{-1}$ and an excited-state population of 16.5 ± 1.7%, which corresponds to intermediate exchange, thus explaining the strong line broadening observed in the methyl-TROSY spectrum (see Figure S5). These values correspond to forward and reverse kinetic rate constants of $84 \pm 8\ s^{-1}$ and $425 \pm 43\ s^{-1}$, respectively. The addition of glucose quenched the millisecond dynamics of the small domain (Figure 2A–C, green curves; see also Figure S4). Some residues belonging to other regions of the enzyme experience dynamics on a faster timescale and are not affected by glucose (Figure 2D).

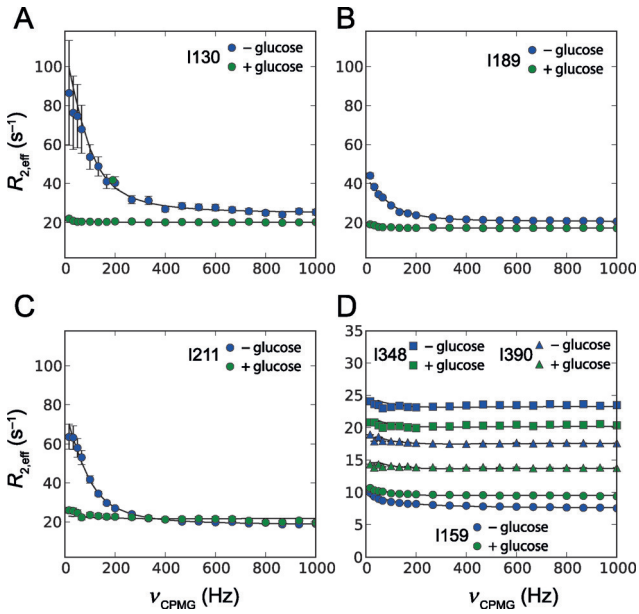

Figure 2. CPMG relaxation dispersion experiments show changes in the methyl dynamics following glucose binding. A–D) Dispersion profiles of residues in the small domain (A–C), disordered loop (D; circles), large domain (D; squares), and hinge region (D; triangles) in the absence (blue) and presence of glucose (green). The data were analyzed with the ChemEx software by numerically solving the Bloch–McConnell equations (see the Supporting Information).[31]

Interestingly, the disordered region spanning residues 151–179 in the small domain with the two NMR reporters I159 and I163 showed essentially no millisecond exchange, with R_{ex} values smaller than 3.8 s^{-1} (see Table S2 in the Supporting Information). Thus, the disordered loop does not sense the intermediate exchange experienced by the other Ile residues of the small domain. This region remains disordered in all dominant substates of unliganded GCK and does not visit other conformations to any significant extent, including the β-hairpin conformation it occupies in the glucose-bound state. By contrast, the other small-domain residues exchange between two or more folded conformational states.

Because of the motional broadening of the NMR spectrum,[32] high-resolution information is unavailable for the conformational substates. However, the CPMG fitting results yield an average proton chemical-shift change of $\Delta\omega = 0.11$ ppm, which is consistent with the average proton chemical-shift change observed between the unliganded and the glucose-bound state of GCK for the small-domain residues that are not in close vicinity to the glucose-binding site (see Table S1). Therefore, these chemical-shift changes, despite their small magnitude, are not incompatible with large conformational changes, similar to those observed between the closed glucose-bound state (PDB ID: 3IDH) and the open, unliganded state (PDB ID: 1V4T).

The turnover rate constant of GCK measured at the temperature at which the NMR spectroscopic experiments were carried out (313 K) is 220 s^{-1} and represents the slowest step in the reaction after glucose and ATP binding have occurred. Kinetic cooperativity is retained at this temperature with a Hill coefficient of 1.6. This turnover value defines the conformational-exchange rates that can contribute to the kinetic cooperativity of the enzyme (Figure 1 A). Conformational exchange processes with a rate constant comparable or smaller (i.e. slower) than the turnover rate constant can cause deviation from Michaelis–Menten kinetics, that is, kinetic cooperativity, since the enzyme has sufficient time between two successive catalytic events to populate the open, inactive state. Return to the active state happens spontaneously with a rate constant of 84 s^{-1}, which may be modulated by the presence of substrates (Figure 3). Interestingly, conformational exchange on the millisecond timescale was largely quenched for an activated variant of GCK (see Figure S6) that does not display significant kinetic cooperativity, thus further corroborating the relevance of the observed wild-type dynamics for kinetic cooperativity.

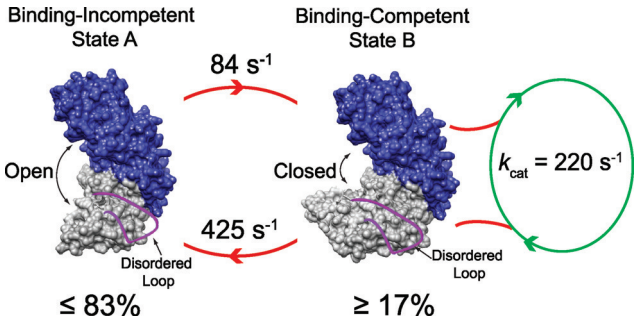

Figure 3. Schematic model for the origin of the kinetic cooperativity of GCK by the interconversion of a binding-competent (right) and binding-incompetent state (left), whereby the loop 151–179 (purple) is disordered in both conformations.

It is possible that the equilibrium dynamic events in the small domain are accompanied by a change in the opening angle between the small and large domains while the loop remains disordered. This possibility could be addressed by characterizing the long-range distance distribution between parts of the two domains that are not in the vicinity of the binding site, for example, by FRET measurements. The population of the binding-incompetent state must be significant to produce the strong kinetic cooperativity effect observed in Figure 1 A. Our estimate of 83 % is consistent with previous global fit analysis of fluorescence spectroscopic studies, which yielded a similar alternative-conformation population.[33] The two-state model used in this study, although sufficient to explain our data, is likely to be an oversimplified representation of the real unliganded glucokinase ensemble.

Our results are consistent with the following model of GCK function: after the phosphorylation of glucose, the β-hairpin 151–179 becomes disordered, which enables the release of phosphorylated glucose and adenosine diphosphate (ADP), whereas the large and small domains remain in a closed conformation. This arrangement is similar to the crystal structure of glucose-bound GCK (PDB ID: 3IDH), except that the loop is disordered. Next, the population of unliganded enzyme gradually transitions from the closed state

to an open state, which is possibly glucose-binding incompetent, on an intermediate timescale ($425\ s^{-1}$), whereas the loop 151–179 remains disordered. The inactive state could be structurally related to the open state (PDB ID: 1V4T), which shows a small-domain topology that differs from that of the closed state (PDB ID: 3IDH).

This study shows how, for this critical enzyme, conformational heterogeneity and conformer interconversion on the relevant timescale provide an elegant means for the precise regulation of its activity. Future studies will focus on the structural and mechanistic role of activating and inactivating mutants of GCK, many of which cause hyperinsulinemia and diabetes.

Keywords: allostery · enzyme catalysis · kinetic cooperativity · NMR spectroscopy · time-resolved conformational dynamics

How to cite: *Angew. Chem. Int. Ed.* **2015**, *54*, 8129–8132
Angew. Chem. **2015**, *127*, 8247–8250

[1] M. Larion, B. G. Miller, *Arch. Biochem. Biophys.* **2012**, *519*, 103–111.
[2] C. Porter, B. G. Miller, *Bioorg. Chem.* **2012**, *43*, 44–50.
[3] F. M. Matschinsky, *Curr. Diabetes Rep.* **2005**, *5*, 171–176.
[4] P. Petit, M. Antoine, G. Ferry, J. A. Boutin, A. Lagarde, L. Gluais, R. Vincentelli, L. Vuillard, *Acta Crystallogr. Sect. D* **2011**, *67*, 929–935.
[5] K. Kamata, M. Mitsuya, T. Nishimura, J. Eiki, *Structure* **2004**, *12*, 429–438.
[6] M. Larion, R. K. Salinas, L. Bruschweiler-Li, B. G. Miller, R. Brüschweiler, *PLoS Biol.* **2012**, *10*, e1001452.
[7] N. M. Motlagh, J. O. Wrabl, J. Li, V. J. Hilser, *Nature* **2014**, *508*, 331–339.
[8] A. C. M. Ferreon, J. C. Ferreon, P. E. Wright, A. A. Deniz, *Nature* **2013**, *498*, 390–394.
[9] C.-J. Tsai, R. Nussinov, *PLoS Comput. Biol.* **2014**, *10*, e1003394.
[10] M. Vogtherr, K. Saxena, S. Hoelder, S. Grimme, M. Betz, U. Schieborr, B. Pescatore, M. Robin, L. Delarbre, T. Langer, K. U. Wendt, H. Schwalbe, *Angew. Chem. Int. Ed.* **2006**, *45*, 993–997; *Angew. Chem.* **2006**, *118*, 1008–1012.
[11] J. Monod, J. Wyman, J. P. Changeux, *J. Mol. Biol.* **1965**, *12*, 88–118.
[12] D. E. Koshland, Jr., G. Némethy, D. Filmer, *Biochemistry* **1966**, *5*, 365–385.
[13] J. Ricard, J.-C. Meunier, J. Buc, *Eur. J. Biochem.* **1974**, *49*, 195–208.
[14] J. Ricard, J. Buc, J.-C. Meunier, *Eur. J. Biochem.* **1977**, *80*, 581–592.
[15] J. Ricard, J. Buc, J.-C. Meunier, *Eur. J. Biochem.* **1977**, *80*, 593–601.
[16] J.-C. Meunier, J. Buc, J. Ricard, *Eur. J. Biochem.* **1979**, *97*, 573–583.
[17] G. R. Ainslie, Jr., J. P. Shill, K. E. Neet, *J. Biol. Chem.* **1972**, *247*, 7088–7096.
[18] K. E. Neet in *Contemporary Enzyme Kinetics and Mechanism* (Ed.: D. L. Purich), Academic Press, New York, **1983**, pp. 267–320.
[19] K. E. Neet, G. R. Ainslie, Jr., *Methods Enzymol.* **1980**, *64*, 192–226.
[20] J. P. Loria, M. Rance, A. G. Palmer, *J. Biomol. NMR* **1999**, *15*, 151–155.
[21] A. G. Palmer, C. D. Kroenke, J. P. Loria, *Methods Enzymol.* **2001**, *339*, 204–238.
[22] D. M. Korzhnev, K. Kloiber, V. Kanelis, V. Tugarinov, L. E. Kay, *J. Am. Chem. Soc.* **2004**, *126*, 3964–3973.
[23] D. Sheppard, R. Sprangers, V. Tugarinov, *Prog. Nucl. Magn. Reson. Spectrosc.* **2010**, *56*, 1–45.
[24] D. M. Korzhnev, K. Kloiber, L. E. Kay, *J. Am. Chem. Soc.* **2004**, *126*, 7320–7329.
[25] V. Tugarinov, V. Kanelis, L. E. Kay, *Nat. Protoc.* **2006**, *1*, 749–754.
[26] D. D. Boehr, D. McElheny, H. J. Dyson, P. E. Wright, *Science* **2006**, *313*, 1638–1642.
[27] G. Bhabha, J. Lee, D. C. Ekiert, J. Gam, I. A. Wilson, H. J. Dyson, S. J. Benkovic, P. E. Wright, *Science* **2011**, *332*, 234–238.
[28] R. Otten, J. Villali, D. Kern, F. A. Mulder, *J. Am. Chem. Soc.* **2010**, *132*, 17004–17014.
[29] V. Tugarinov, P. M. Hwang, J. E. Ollerenshaw, L. E. Kay, *J. Am. Chem. Soc.* **2003**, *125*, 10420–10428.
[30] A. J. Baldwin, T. L. Religa, D. F. Hansen, G. Bouvignies, L. E. Kay, *J. Am. Chem. Soc.* **2010**, *132*, 10992–10995.
[31] P. Vallurupalli, G. Bouvignies, L. E. Kay, *J. Am. Chem. Soc.* **2012**, *134*, 8148–8161.
[32] M. Larion, R. K. Salinas, L. Bruschweiler-Li, R. Brüschweiler, B. G. Miller, *Biochemistry* **2010**, *49*, 7969–7971.
[33] M. Larion, B. G. Miller, *Biochemistry* **2010**, *49*, 8902–8911.

Received: February 7, 2015
Revised: April 15, 2015
Published online: May 26, 2015

